Nano Energy 24 (2016) 78–86

Contents lists available at ScienceDirect

Nano Energy

journal homepage: www.elsevier.com/locate/nanoen

Asymmetric supercapacitors with metal-like ternary selenides and porous graphene electrodes

Chuan Xia, Qiu Jiang, Chao Zhao, Pierre M. Beaujuge, Husam N. Alshareef*

Materials Science and Engineering, King Abdullah University of Science and Technology, (KAUST), Thuwal 23955-6900, Saudi Arabia

ARTICLE INFO

Article history:
Received 7 March 2016
Received in revised form
9 April 2016
Accepted 12 April 2016
Available online 14 April 2016

Keywords:
Nickel cobalt selenide
Porous graphene film
Asymmetric supercapacitor
High conductivity

ABSTRACT

Asymmetric supercapacitors provide a promising approach to fabricate capacitive energy storage devices with high energy and power densities. In this work, asymmetric supercapacitors with excellent performance have been fabricated using ternary $(Ni, Co)_{0.85}Se$ on carbon fabric as binder-free positive electrode and porous free-standing graphene film as negative electrode. Owing to their metal-like conductivity ($\sim 1.67 \times 10^6$ S m^{-1}), significant electrochemical activity, and superhydrophilic nature, our nanostructured ternary nickel cobalt selenides result in a much higher areal capacitance (2.33 F cm^{-2} at 4 mA cm^{-2}), better rate performance and cycling stability than their binary selenide equivalents, and other ternary oxides and chalcogenides. Those hybrid supercapacitors can afford impressive areal capacitance and stack capacitance of 529.3 mF cm^{-2} and 6330 mF cm^{-3} at 1 mA cm^{-2}, respectively. More impressively, our optimized asymmetric device operating at 1.8 V delivers a very high stack energy density of 2.85 mW h cm^{-3} at a stack power density of 10.76 mW cm^{-3}, as well as 85% capacitance retention after 10,000 continuous charge–discharge cycles. Even at a high stack power density of 1173 mW cm^{-3}, this device still deliveries a stack energy density of 1.19 mW h cm^{-3}, superior to most of the reported supercapacitors.

1. Introduction

While batteries keep our portable devices working throughout the day, they take hours to recharge. For rapid power delivery and recharging, supercapacitors, also called as electrochemical capacitors, hold great promise [1]. In spite of their fast rate of charge and discharge, supercapacitors also demonstrate excellent reusability, safe operation and low maintenance cost. Hence, they have been widely used independently as back-up power devices or coupled with batteries in hybrid electronic vehicles [2]. However, supercapacitors have low energy density which greatly hinders their practical applications in various electronic smart devices. Thus, there is an urgent need to increase the energy density of supercapacitors without compromising their power density. There are two key parameters which can be used to improve the energy density of supercapacitors: increasing the capacitance of the electrode material, *C*, or the operation voltage window, *V*, or both, since the energy stored is proportional to CV^2 [3].

Very recently, it has been realized that asymmetric supercapacitors (ASCs) can be an alternative and efficient pathway (compared with symmetric supercapacitors), to extend the output voltage of supercapacitors beyond the thermodynamic limit of $\sim$1.23 V in aqueous solutions. This increase in operating voltage led to significant enhancement of energy density of ASCs. These ASCs typically consist of a Faradic positive electrode as the energy source, and a capacitor-type negative electrode as the power source [4,5]. For ASCs, using different negative and positive electrode materials with well-separated potential windows widens the usable cell voltage, while simultaneously offering advantages of both supercapacitors (power density, rate, lifespan) and batteries (energy density) [4,6]. For example, Gao et al. fabricated an asymmetric supercapacitor using graphene hydrogel and MnO_2, which possessed a wide potential window of 2.0 V and exhibited an energy density of 23.2 W h kg^{-1} with a power density of 1.0 kW kg^{-1} [7]. Zhou et al. showed that the $NiMoO_4$//activated carbon hybrid supercapacitor could deliver an energy density of 45.6 W h kg^{-1} at 674 W kg^{-1} with a voltage of 1.62 V [8]. However, to measure the energy density of supercapacitors in a more practical way, it has recently been suggested that the stack energy density (in units of mW h cm^{-3}) involving the entire supercapacitor components should be reported instead of the gravimetric one (which only considers the mass-loading of active materials in units of W h kg^{-1}) to realistically evaluate supercapacitor devices [3,9,10]. Replacing aqueous electrolytes with organic electrolytes or ionic liquids is another strategy commonly investigated for the design of high-voltage supercapacitors.

* Corresponding author.
E-mail address: husam.alshareef@kaust.edu.sa (H.N. Alshareef).

http://dx.doi.org/10.1016/j.nanoen.2016.04.012
2211-2855/

However, non-aqueous electrolytes always suffer from limited ionic conductivity, more cost, and environmental risks in case of leakage [7]. Therefore, the above-mentioned disadvantages make such an approach practically undesirable.

On the other hand, in order to improve the cell capacitance (another key parameter to enhance the capability), it is highly desirable to explore novel electrode materials with high specific capacitance and promising conductivity. In this regard, pseudocapacitive or Faradic MnO_2 [11], Co_3O_4 [12], $Ni(OH)_2$ [13] and some conducting polymers [14,15] have been developed for advanced supercapacitor positive electrode materials. Yet, their low electrical conductivity and/or poor cycling stability make their electrochemical performance mostly inferior. Tremendous efforts have been exerted to overcome these limitations, including preparation of hybrid carbon/oxide electrodes [16], deposition nanostructured electroactive materials into a conductive network [8,14], and so on. As previously demonstrated by our group [17–19] and other researchers [20–24], one main direction to improve the performance of electrode materials is the rational design of three-dimensional (3D) nanostructured ternary transition metal chalcogenides such as metallic $NiCo_2S_4$ [25]. Due to their superior electrical conductivity, richer electrochemical redox reactions, better chemical stability and shorter diffusion path for both electrons and electrolyte ions, 3D ternary metal chalcogenides show promising performance for supercapacitor positive electrodes. In particular, nickel/cobalt-based chalcogenides are considered as ideal candidates due to their low cost, abundance, and environmental friendliness. While the high-performance ternary chalcogenide electrode has been studied, most studies have used low mass-loading for positive electrode materials (typically 0.5–1 mg cm^{-2}), which makes it hard to predict how these materials will perform in real applications. On the negative side of supercapacitors, graphene has been explored extensively because of its large theoretical surface area, excellent conductivity and chemical stability. Various pioneering studies point out that the porous and yet densely packed graphene electrodes with large ion-accessible surface areas, and low ion transport resistance are crucial to the realization of graphene-based high-energy supercapacitors [9,26]. Hence, we believe that graphene film with in-plane and out-of-plane pores, and carefully controlled packing density would be very suitable negative electrode material for ASCs.

Although considerable work has been done on ASCs, one remaining challenge is to combine appropriate electrode materials working in well-separated potential windows in the same electrolyte to achieve high operating voltage and consequently high energy density. In this article, we report a simple approach to achieve high-performance 3D ternary nickel cobalt selenide ($(Ni,Co)_{0.85}Se$) supercapacitor positive electrode with high mass loading ($\sim$5.63 mg cm^{-2}). On the negative side, we use porous graphene films prepared by chemical activation. The fabricated $(Ni,Co)_{0.85}Se$//porous graphene ASCs exhibit outstanding electrochemical performance with total mass-loading of $\sim$10 mg cm^{-2}. Specifically, the optimized ASCs showed an areal capacitance of 530 mF cm^{-2} at 1 mA cm^{-2} and a maximum stack energy density (calculated based on entire device thickness) of 2.85 mW h cm^{-3} at the power density of 10.8 mW cm^{-3}. Furthermore, such an asymmetric supercapacitor displayed impressive cycling stability (85% retention after 10,000 cycles at 20 mA cm^{-2}) at a voltage of 1.8 V.

2. Experimental section

2.1. Preparation of $(Ni, Co)_{0.85}Se$

The self-sacrificial template of NiCo-precursor nanoarrays were firstly fabricated using a hydrothermal method. Typically, 8 mmol of $Co(NO_3)_2 \cdot 6H_2O$, 4 mmol $Ni(NO_3)_2 \cdot 6H_2O$ and 15 mmol of urea were dissolved in 80 ml deionized water to form a clear pink solution. This solution was subsequently transferred into a Teflon-lined autoclave with a piece of carbon fabric (CFC) immersed into the solution and kept at 120 °C for 6 h. After cooling down to the room temperature, the precursor coated carbon fabric was obtained and washed with deionized water and ethanol. Afterwards, the Ni-Co-precursors were chemically converted in situ into $(Ni, Co)_{0.85}Se$ by 1.0 M fresh NaHSe selenization. In a typical procedure, one piece of as-prepared NiCo-precursor, 38 mL Argon saturated deionized water and 2 mL of fresh prepared 1 M NaHSe solution were loaded into a Teflon lined stainless steel autoclave. The autoclave was heated at 160 °C for 24 h, and then cooled to room temperature naturally. The final product was washed and dried in vacuum at 60 °C. Note that 1.0 M fresh NaHSe was prepared by mixing $\sim$0.16 g $NaBH_4$, $\sim$0.16 g Se powder and 2 mL Argon saturated deionized water under inert gas protection according to the following equation: $4NaBH_4 + 2Se + 7H_2O = 2NaHSe + Na_2B_4O_7 + 14H_2$.

2.2. Preparation of porous graphene film

The in-plane porous graphene oxide was prepared according to previous report [27]. Afterwards, the highly porous graphene film was obtained by vacuum filtration as described elsewhere [9,26,27].

2.3. Fabrication of $(Ni, Co)_{0.85}Se$//porous graphene film asymmetric supercapacitors

The as-synthesized $(Ni, Co)_{0.85}Se$ was directly used as positive electrode. Thicker graphene films were made through stacking a certain number of graphene films together in a face-to-face manner in order to reach a charge balance in negative and positive electrode. The thicker graphene film was then attached to the carbon cloth and used as a negative electrode. Note that that carbon cloth in negative electrode also acted as the current collector. A 1.0 M KOH solution was used as electrolyte and a porous polymer membrane was used as the separator (Celgard 3501). The asymmetric devices were assembled in pouch cells by sealing them into plastic bags to avoid evaporation of the aqueous electrolyte during long-time measurement. For a typical asymmetric device, the total mass loading of the active material is $\sim$10 mg cm^{-2} with a stack thickness of $\sim$0.84 mm.

2.4. Characterization

X-ray diffraction (XRD) spectra were collected by a Bruker diffractometer (D8 Advance) with Cu Kα radiation, $\lambda = 1.5406$ Å. The morphology and microstructure of the samples were characterized by SEM (Nova Nano 630, FEI) and HRTEM (Titan 80; 300 kV for selenides and 80 kV for graphene). Energy-dispersive spectroscopy (EDS) elemental analysis were performed on the same instrument in scanning TEM (STEM) mode. The contact angle was imaged using Theta/Attension optical tensiometer. XPS spectra were recorded on Kratos AXIS Ultra DLD.

2.5. Electrochemical measurements

The electrochemical tests were conducted at room temperature in a VMP3 electrochemical workstation (Bio-Logic) by the techniques of electrochemical impedance spectroscopy (EIS), cyclic voltammetry (CV) and galvanostatic charge–discharge (CD). 1.0 M KOH was used as the electrolyte for all supercapacitor devices. In 3-electrode measurements, selenide-covered CFC or graphene film directly used as working electrode with a Pt counter electrode and

a saturated Ag/AgCl reference electrode. Electrical impedance spectroscopy was recorded under the following conditions: ac voltage amplitude 5 mV, frequency ranges 10^5–0.1 Hz and open circuit.

The energy density was calculated from the galvanostatic discharge (CD) curves:

$$E_{areal} = \frac{I\int_{t(U_{max})}^{t(U_{min})} U(t)dt}{A}$$

$$E_{stack} = \frac{I\int_{t(U_{max})}^{t(U_{min})} U(t)dt}{T}$$

where I is the constant current for charge–discharge and $t(U_{max})$ and $t(U_{min})$ are the times at the maximum and minimum voltage during a discharge process. A is the area of the entire electrode and T is the entire volume of our as-prepared ASCs.

Power density:

$$P=\frac{E}{t}$$

While capacitance can be calculated from the following equation:

$$C = \frac{2E}{U_{max}{}^2}$$

where U_{max} is the voltage window (1.8 V) applied during the charge–discharge measurements.

3. Results and discussion

Nanostructured ternary nickel cobalt selenides were directly grown on carbon fabric (CFC) substrate in order to avoid the addition of polymer binders and conductive agents which are non-desirable for high-performance supercapacitors. In addition, direct growth on CFC results in lower contact resistance between the electroactive materials and the CFC current collector which facilitates the electron transfer from electrochemical reaction sites to the collector [8]. As a result, we believe that such a direct fabrication method is superior to the conventional slurry process that is often used to prepare supercapacitor electrodes. Typical X-ray diffraction (XRD) pattern (Fig. 1A) and energy-dispersive spectroscopy (EDS) analysis (Fig. S1A) support the formation of hexagonal Ni doped $Co_{0.85}Se$ (JCPDS 52-1008). Moreover, our XPS survey spectrum analysis confirms the successful introduction of Ni into $Co_{0.85}Se$ lattice (Fig. S1B). It is well known that the cations in cobalt based oxides and chalcogenides can be easily substituted by nickel ions without significantly distorting their crystal structures [28]. Additionally, the introduction of nickel ions into cobalt compounds might cause a significant enhancement of electrical conductivity (conductivity of $NiCo_2O_4$ is at least 100 times higher than Co_3O_4) [23]. To show this conductivity enhancement effect, we directly measured the electrical transport properties of the as-prepared $Co_{0.85}Se$ and $(Ni, Co)_{0.85}Se$ from the temperature dependence of resistivity using pellets compressed from chemically prepared nanopowders, along with $NiCo_2O_4$ as control. The data in Fig. S2 clearly shows that the electrical conductivity of $(Ni, Co)_{0.85}Se$ is about 2 times higher than that of pure $Co_{0.85}Se$ at room temperature. Furthermore, unlike the typical semiconductor

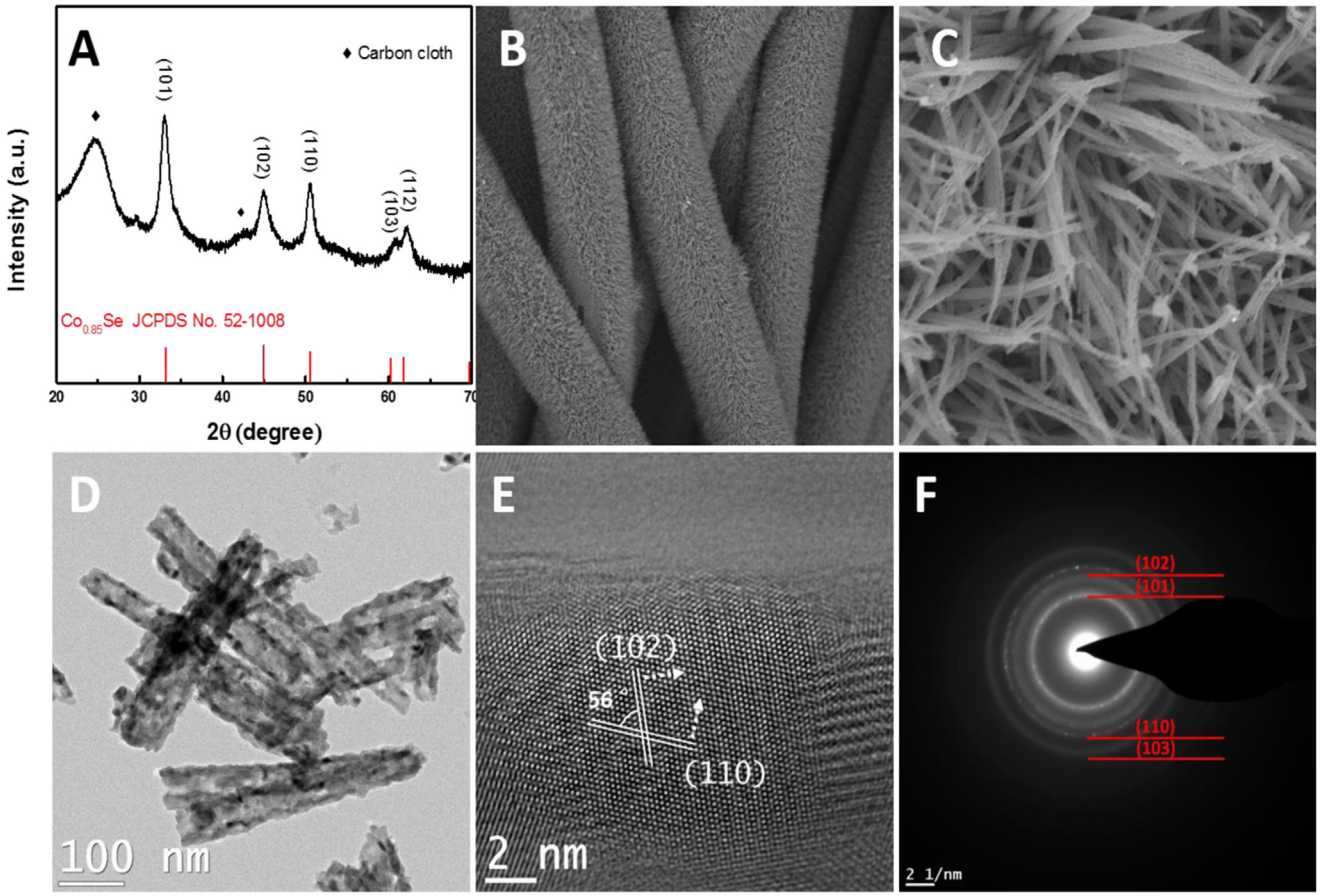

Fig. 1. (A) The representative XRD pattern for as-prepared $(Ni, Co)_{0.85}Se$ nanotube arrays on CFC. The typical (B, C) FESEM and (D, E) TEM images for as-prepared $(Ni, Co)_{0.85}Se$ nanotubes as well as (F) corresponding SAED pattern.

$NiCo_2O_4$, the resistivity of the selenides actually increases linearly with temperature from of 2 to 300 K, indicating their metallic nature [25]. Such an excellent conductivity (1.67×10^6 S m^{-1} compared with 9.1×10^6 S m^{-1} for Pt) can facilitate the charge transfer process and minimize the voltage drop in the electrode, which are highly desired features for high-rate supercapacitor electrodes. Furthermore, our previous study has clearly demonstrated that the (Ni, Co)$_{0.85}$Se nanostructure offers much higher electrochemical active surface area and electrochemical activity than $Co_{0.85}Se$ [29]. Thus, this ternary (Ni, Co)$_{0.85}$Se shows clear advantages over binary $Co_{0.85}Se$ as supercapacitor electrode.

The morphology and microstructure of as-obtained (Ni,Co)$_{0.85}$Se was examined by field-emission scanning electron microscopy (FESEM) and transmission electron microscopy (TEM). The panoramic and close-up FESEM images (Fig. 1B and C) show that the (Ni,Co)$_{0.85}$Se consists of closely packed and vertically aligned nanotube arrays on CFC. The formation of the hollow interior is related to the diffusion process of the cations, known as the Kirkendal effect [30]. Further, the corresponding TEM and high-angle annular dark-field scanning TEM (HAADF-STEM) images (Figs. 1D and S3) reveal that the surface of (Ni, Co)$_{0.85}$Se nanotube is very rough and highly porous. As we know, the woven conductive CFCs demonstrate macroporous nature themselves (Fig. S4) which can serve as an excellent scaffold for the deposition of electroactive materials. As a result, the ternary (Ni, Co)$_{0.85}$Se electrodes offer a combination of macroporosity (from the carbon fiber) and mesoporosity from the nanostructure of the ternary chalcogenide nanowires. This combination is believed to facilitate the electrolyte ion trapping and access to electrochemical active sites, which reduces the electrolyte ion diffusion distance during the charge–discharge process. Similar design of nanoporous materials on macroporous substrate have previously shown as promising integrated electrode for supercapacitor devices [17,31]. The high-resolution TEM in Fig. 1E shows clear well-defined lattice fringes for (Ni, Co)$_{0.85}$Se, indicating a high degree of crystallinity. The crystal lattice with a spacing of ~0.2 nm and ~0.18 nm corresponds to the (102) and (110) planes of $Co_{0.85}Se$, respectively. Further, the selected area electron diffraction (SAED) of as-prepared (Ni, Co)$_{0.85}$Se (Fig. 1F) shows its polycrystalline nature, in agreement with the XRD result.

Cycling voltammetry (CV) is generally used to characterize the capacitive behavior of an electrode material. Fig. 2A shows the CV curves of as-prepared (Ni, Co)$_{0.85}$Se at different scan rate in 1.0 M KOH electrolyte. All the CV plots here exhibit a pair of pronounced redox peaks, which correspond to the typical faradic reaction among transformation of Ni^{2+}/Ni^{3+} and $Co^{2+}/Co^{3+}/Co^{4+}$ in alkaline solution [17,18,23]. The symmetric characteristic of the anodic and cathodic peaks indicates the excellent reversibility of selenide electrodes. Additionally, Fig. 2B shows that a linear relationship exists between the potential of the anodic and cathodic peaks and the square root of scan rate. This linear behavior indicates the dominance of diffusion-controlled electrode reactions, which reveals that the energy storage in our selenide electrode is mainly based on the faradic reactions rather than electric double-layer physiadorption. Likewise, the voltage plateaus observed in the galvanostatic charge–discharge (CD) profiles also confirm the

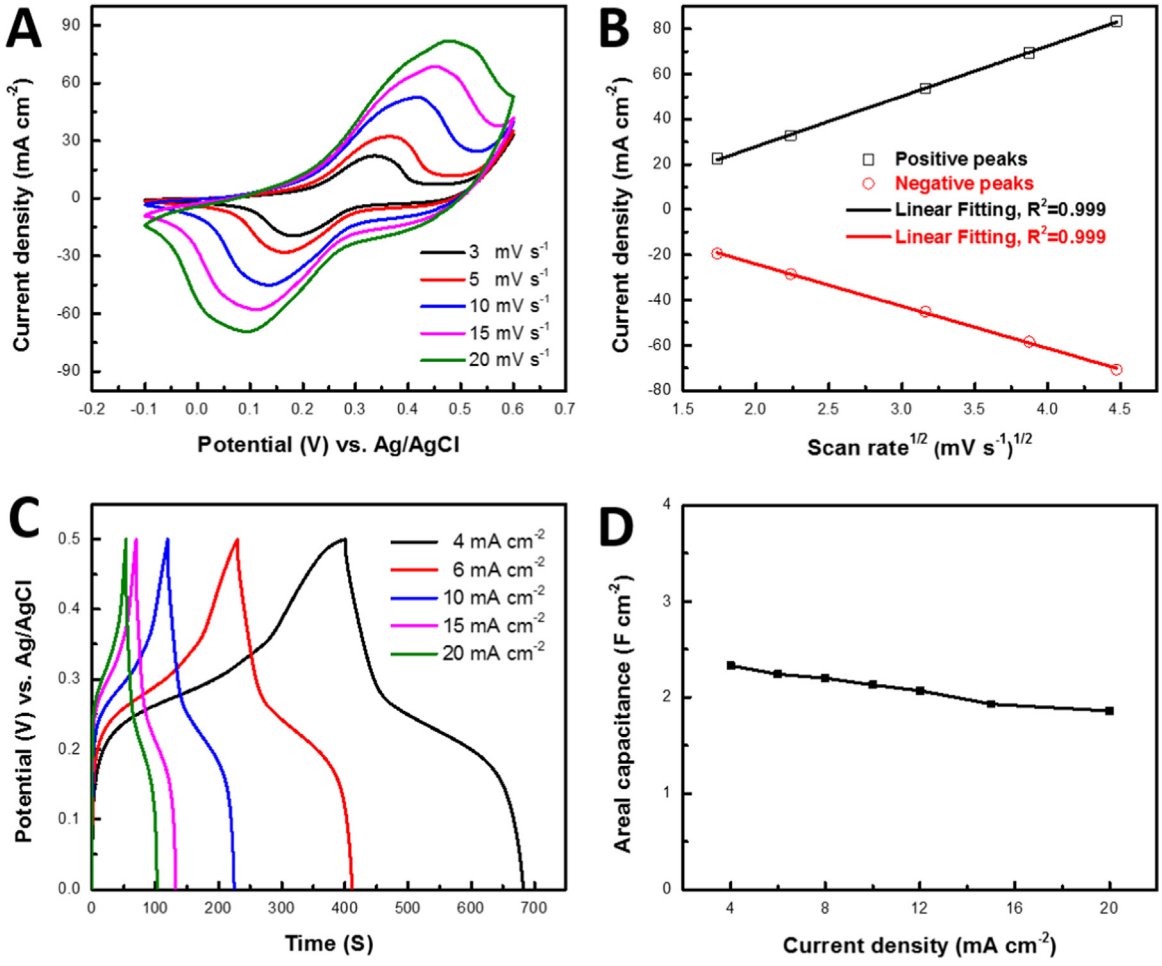

Fig. 2. (A) Cyclic voltammetry curves of (Ni, Co)$_{0.85}$Se at different scans; and (B) plots of anodic and corresponding cathodic peak densities presented in (A) versus the square root of scan rate. (C) Galvanostatic charge–discharge profiles of (Ni, Co)$_{0.85}$Se with different current densities, and (D) corresponding discharge areal capacitance.

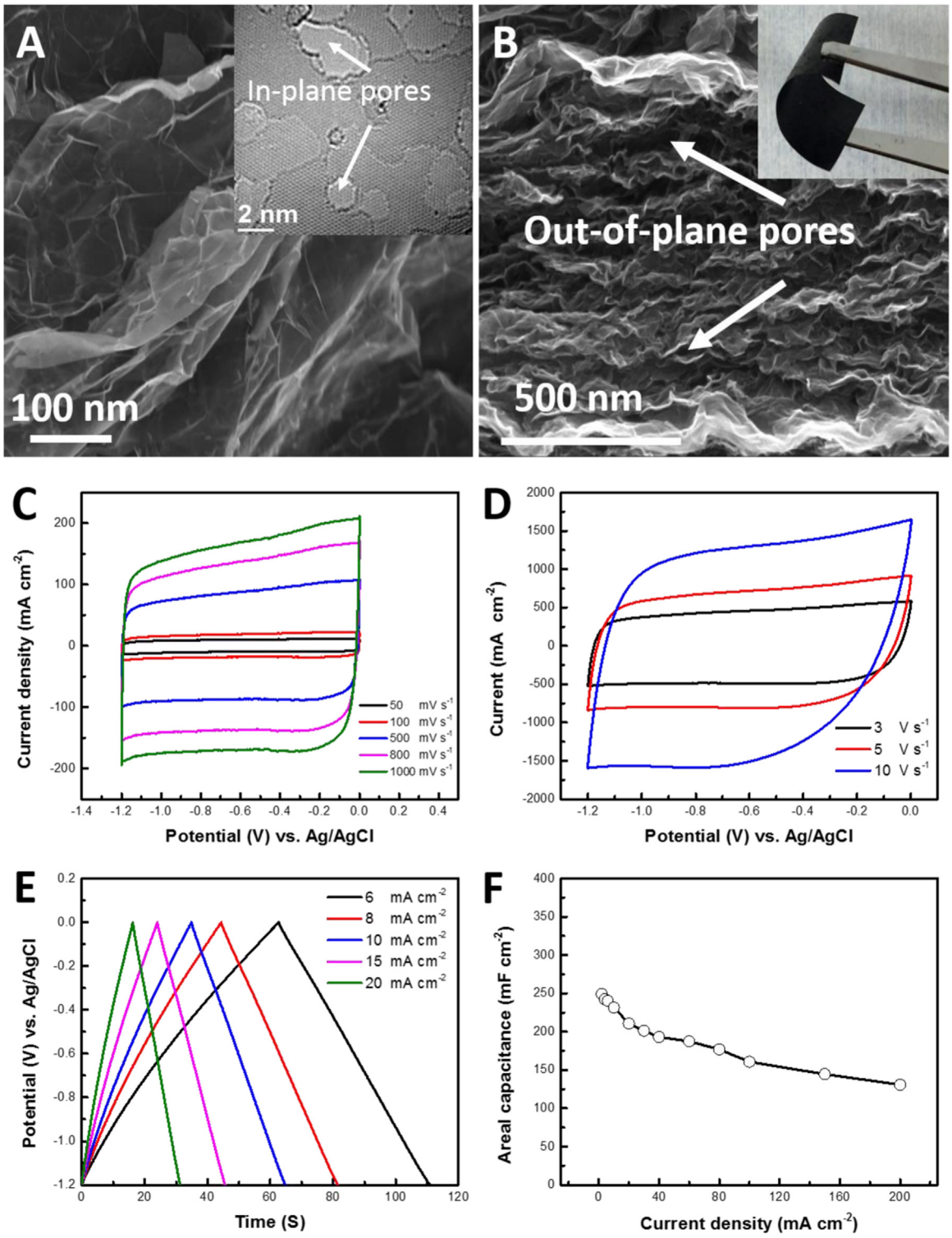

Fig. 3. (A) FESEM and (inset) TEM images of as-obtained porous graphene. (B) Typical cross-section FESEM image of vacuum filtered porous graphene film. The inset of (B) shows the digital photo of porous graphene film. (C, D) Cyclic voltammetry plots of porous graphene film at different scans. (E) Plots of galvanostatic charge–discharge profiles of porous graphene film with different current densities, and (F) corresponding discharge areal capacitance.

faradic process (Fig. 2C), which is consistent with the electrochemical behavior of the CV curves. The negligible voltage (IR) drop observed in the CD curves is attributed to the excellent conductivity of (Ni, $Co)_{0.85}Se$ (1.67×10^6 S m^{-1}) which result in prominent rate capability. The CD curves of as-synthesized (Ni, $Co)_{0.85}Se$ nanotube arrays are nearly symmetric in nature, which reveals the highly reversible nature of our electrodes [30]. As summarized in Fig. 2D, the areal capacitance of (Ni, $Co)_{0.85}Se$ electrode was calculated to be 2.33 F cm^{-2} and 1.86 F cm^{-2} at current density of 4 mA cm^{-2} and 20 mA cm^{-2}, respectively. Impressively, the areal capacitance of our ternary electrode is ~2.5-folds higher than previously reported binary $Co_{0.85}Se$ supercapacitor electrode at same current density of 4 mA cm^{-2} [30]. Besides, our ternary electrode showed an enhanced rate capability when compared to binary $Co_{0.85}Se$. Specifically, 80% of the capacitance retention takes place when the current density increase

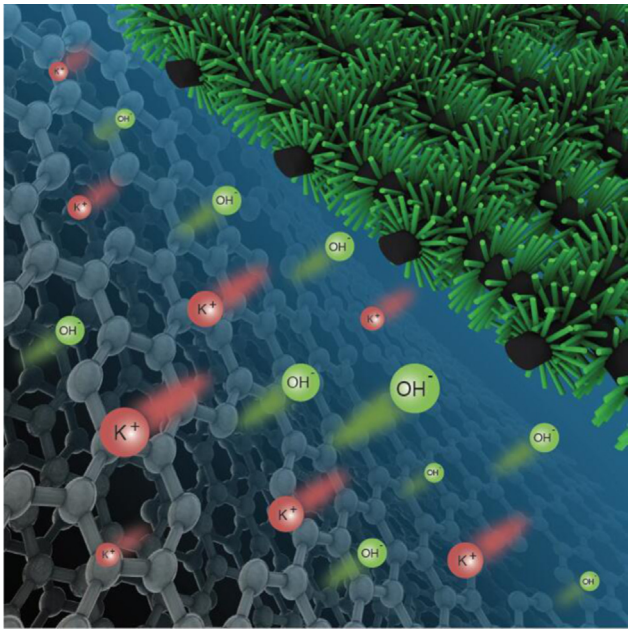

Fig. 4. Schematic of the design of asymmetric supercapacitors by applying nickel cobalt selenide arrays on carbon cloth as a positive electrode and porous graphene film as a negative electrode.

from 4 mA cm^{-2} from 20 mA cm^{-2} whereas that of $Co_{0.85}Se$ is only ~64% [30]. As we mentioned above, such an improvement is probably related to their remarkable electrical conductivity and nanostructure. What is more, it is worthwhile to note that the areal capacitance reported here is higher than the values reported so far for pseudocapacitive oxides/hydroxides/chalcogenides, such as $NiCo_2O_4$ nanoneedles (~1.44 F cm^{-2} at 2.78 mA cm^{-2}) [32], $Co_xNi_{1-x}(OH)_2/NiCo_2O_4$ (~2.3 F cm^{-2} at 2 mA cm^{-2}) [33], $CoNi_2S_4$ nanosheets arrays (~1.12 F cm^{-2} at 4 mA cm^{-2}) [17], and $MnO_2/NiCo_2O_4$ (~2.01 F cm^{-2} at 2 mA cm^{-2}) [34]. The excellent electrochemical capacitive performance of our ternary selenide electrode can be attributed to the following facts: (1) the fabrication process of our integrated electrodes prevents the addition of "dead volume" from binder and conductive agent, which provides a superb highways for fast electron transportation and electrolyte ion diffusion; (2) the metallic nature of $(Ni, Co)_{0.85}Se$ reduces the equivalent series resistance (ESR) and ensures fast electron transport to the current collector, thereby enhancing the rate capability; (3) the superhydrophilic nature of $(Ni, Co)_{0.85}Se$-covered CFC (supporting videos) means the aqueous solution easily spreads on the entire surface (external and internal) of our integrated electrode, hence boosting the electrolyte ion trapping and access to the active sites; (4) the 3D nanostructured porous morphology shortens the diffusion path for mass transport and enhances the concentration of active sites. Overall, because of the promising performance of our ternary positive electrode material, we decided to fabricate asymmetric supercapacitor devices with a suitable negative electrode material with well-separated operating voltage window compared to $(Ni, Co)_{0.85}Se$ positive electrode.

Supplementary material related to this article can be found online at http://dx.doi.org/10.1016/j.nanoen.2016.04.012.

As a well-known member of carbon family, graphene has emerged as a promising negative electrode material for supercapacitors because of its extraordinary conductivity, large theoretical surface area (2630 m^2 g^{-1}) and excellent chemical stability. However, the exploitation of graphene-based bulk material faces a key scientific and technical challenge. Apart from other carbonaceous materials, the performance of graphene-based materials is strongly affected by the way the individual sheets are arranged. The strong π–π interaction between the graphene layers is conducive to restacking of the sheets, resulting in significantly compromised graphene electrodes. Previous reports have shown that water, the very "soft" matter, can serve as an effective "spacer" to prevent the restacking of chemically converted graphene (CCG) sheets [9,26]. The CCG film-like electrodes have shown outstanding performance in energy storage applications, where large-scale application of graphene in bulk film form appears to be close to the market [17,26]. Further studies showed that the in-plane pores in individual graphene sheet can efficiently boost the mass transportation and expanded electrode/electrolyte contact areas in such a graphene film electrode, which are favorable for high-performance supercapacitor electrode [4,27]. In this respect, self-supported porous graphene film would be very suitable negative electrode for construction of an advanced asymmetric supercapacitors.

The porous graphene was prepared according to previous reports [26,27]. FESEM image (Figs. 3A and S5A) of the as-obtained graphene reveals that numerous winkled and folded regions are exhibited on the sheets. Such a rough surface produces higher surface area which is particularly favorable for carbonaceous materials. We can see from Figs. 3A and S5B, C that considerable mesopores are randomly distributed on the individual graphene sheets with a thickness of few atomic layers. Moreover, the typical FESEM image (Fig. 3B) of our porous graphene film demonstrates the presence of abundant out-of-plane pores inside this bulk electrode, which was prepared by vacuum filtration [26]. The large out-of-plane macropores originate from graphene sheets where the aqueous electrolyte serves as the "spacer". As we mentioned above, such a nanoarchitecture with both mesopores and macropores present, is highly desirable for energy storage devices. When evaluated as supercapacitor negative electrode, as displayed in Fig. 3C, the porous graphene film shows typical rectangular CV curves. It can be clearly seen that all the CV curves retained perfect rectangular shapes as the scan rate was increased from 50 to 1000 mV s^{-1}, implying the improved mass transport, efficient electron transfer, and small ESR. It is very important to notice that even when the scan rate goes up to 10,000 mV s^{-1} (Fig. 3D), such a porous electrode still could keep a quasi-rectangular shape. This result clearly indicates the high rate performance of our porous graphene film which is very important for practical supercapacitor applications [30]. The capacitive performances of these graphene negative electrodes were further studied by galvanostatic charge–discharge measurements, as shown in Fig. 3E. The symmetrical triangle feature and negligible IR drop at any current densities reconfirms its low internal resistance and typical capacitor behavior. As summarized in Fig. 3F, in a prolonged voltage window of 1.2 V, the porous graphene film electrode not only offers a high areal capacitance (249.1 mF cm^{-2} at 2 mA cm^{-2}) but also maintains superior rate performance. In spite of the increase in the current density by a factor of 100, ~53% retention (131 mF cm^{-2} at 200 mA cm^{-2}) of initial capacitance is observed. Notably, all the measurements indicate that this graphene film is ideal as a negative electrode for advanced asymmetric supercapcitors.

Our hybrid supercapcitors are constructed with ternary $(Ni,Co)_{0.85}Se$ as positive electrode, porous graphene film as negative electrode, and 1.0 M KOH as electrolyte which is schematically illustrated in Fig. 4. To optimize the performance of the ASCs, the mass loading of the two electrode was balanced before making the full cell using the following equation [17]:

$$\frac{m_+}{m_-} = \frac{C_{s-} \cdot \Delta V_-}{C_{s+} \cdot \Delta V_+}$$

where m is the mass, C_s is the specific capacitance and ΔV is the voltage range for positive electrode (+) and negative electrode

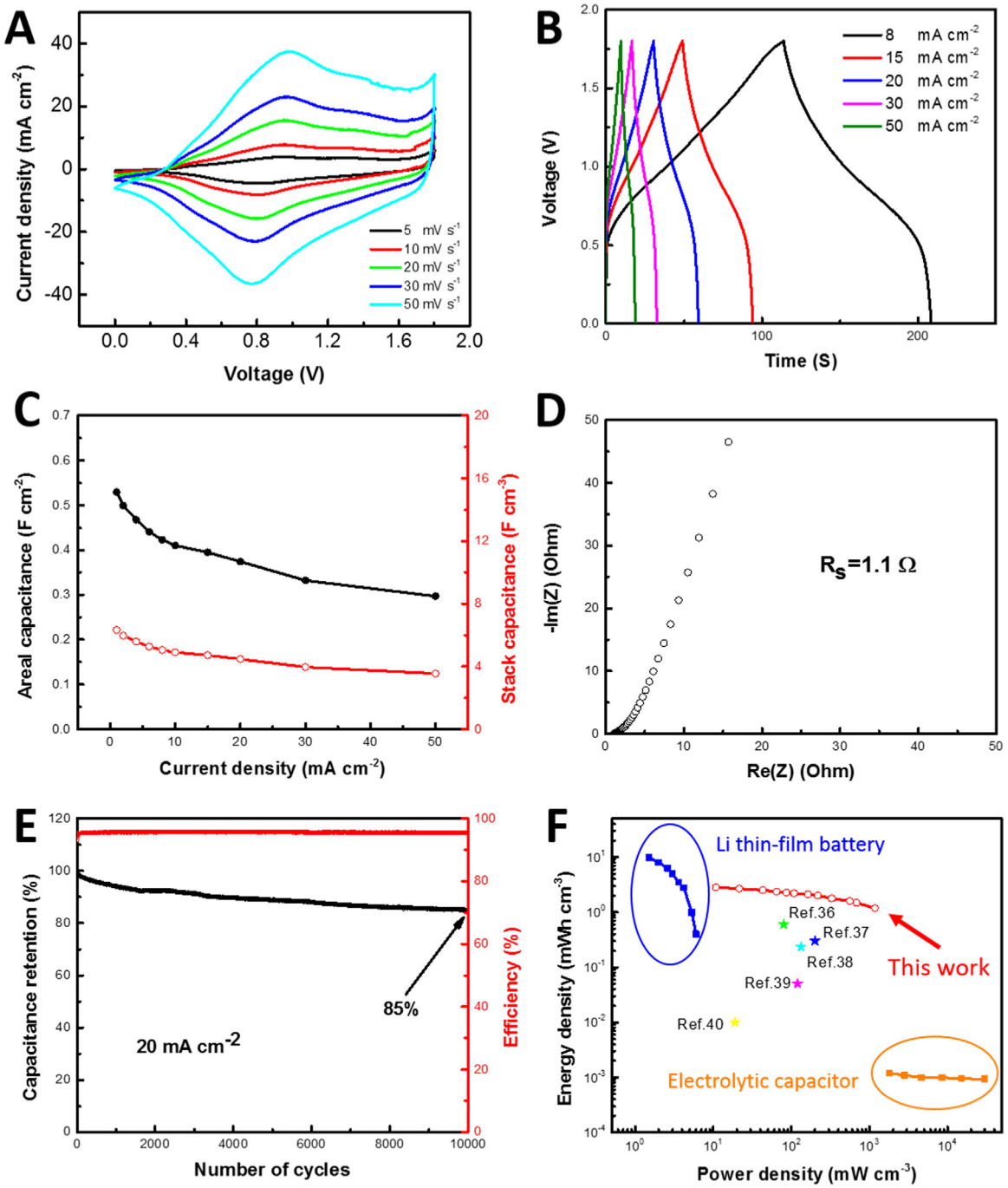

Fig. 5. Electrochemical performance of the (Ni, Co)$_{0.85}$Se//porous graphene film ASC. (A) Cyclic voltammetry curves; (B) plots of galvanostatic charge–discharge profiles; (C) areal and stack capacitance; (D) Nyquist plot; (E) cycling stability performance and (F) Ragone plot.

(−) electrodes, respectively. According to their respective potential windows, the operating potential window of the full cell was determined to 1.8 V (Fig. S6). CV was first used to estimate the electrochemical behavior of balanced (Ni,Co)$_{0.85}$Se//porous graphene film ASC. As shown in Fig. 5A, a pair of distinct peaks under different scan rates could be observed, corresponding to the redox reactions of selenide electrode in basic electrolyte. Taking advantages of their porous nature and intrinsically high conductivity of both positive and negative electrodes, the shifting of redox peaks at high scan rate of the ASC is small, indicating superior rate performance. Moreover, CD measurements were also performed using different current densities in a potential window of 0–1.8 V (Fig. 5B). The nearly symmetric CD profiles with a Coulumbic efficiency of >98% and very small voltage drops also indicate nearly ideal supercapacitor performance with a rapid *I–V* response. Further, the areal capacitances of the (Ni,Co)$_{0.85}$Se//porous graphene film ASCs were calculated and summarized in Fig. 5C. To be specific, this ASC shows impressive areal capacitance and stack capacitance of 529.3 mF cm^{-2} and 6330 mF cm^{-3} at 1 mA cm^{-2}, respectively. This value is significantly better than previously report binary cobalt selenide//activated carbon ASCs (330 mF cm^{-2} at 1 mA cm^{-2}) [30]. And impressively, these devices could reaches 297 mF cm^{-2} and 3550 mF cm^{-3} at a very high current density of 50 mA cm^{-2}, meaning ~56.1% capacitance retention in spite of the increase in current density by a factor of 50. Note that such a high areal capacitance of our ASCs demonstrates their good

capability to store enough energy in a confined area. Electrochemical impedance spectroscopy (EIS) was further employed to investigate the ASC. The ESR of the asymmetric device is mere ~1.1 Ω as shown in the Nyquist plot (Fig. 5D), which also shows negligible charge transfer resistance (R_{ct}). This is due to the hydrated surface and highly porous nanoarchitecture of both negative and positive electrode materials, which minimizes the contact resistance between electrodes and electrolyte.

In view of the fact that cycling stability has always been regarded as a crucial role in ASC applications, the long-term cycling test was carried out for 10,000 CD cycles at a high current density of 20 mA cm^{-2} (Fig. 5E). Notably, our ASC is capable of retaining ~85% of the initial discharge capacitance after 10,000 cycles, showing an impressive lifespan. In addition, such cycling performance is highly competitive with those of some other ASCs, such as $Ni(OH)_2$//activated carbon (82% retention after 1000 cycles) [35], MnO_2@graphene//graphene (79% retention after 1000 cycles) [36], Ni(OH)–CNT//activated carbon (83% retention after 3000 cycles) [37], $Ni_xCo_{3-x}O_4$//activated carbon (82.8% retention after 3000 cycles),[38] and Ni–Co sulfide//activated carbon (73.1% retention after 3000 cycles) [39]. To further illustrate the electrochemical performance of our asymmetric cells, Ragone curve is plotted in Fig. 5F based on the stack energy density and stack power density. In order to fairly and accurately reveal their energy storage performances, the values of high-energy lithium thin-film battery (4 V/500 μA h) [40] and high-power aluminum electrolytic capacitor (3 V/300 μF) [41] are also included as control. The ASC cell shows a high stack energy density of 2.85 mW h cm^{-3} at a power density of 10.76 mW cm^{-3}. Even at a high power density of 1173 mW cm^{-3}, this device still deliveries a stack energy density of 1.19 mW h cm^{-3}, superior to most of the reported supercapacitors including VOx//VN (0.6 mW h cm^{-3} at 80 mW cm^{-3}) [42], H–TiO_2@MnO_2//H–TiO_2@C (0.30 mW h cm^{-3} at 200 mW cm^{-3}) [43], ZnO@MnO_2//graphene (0.234 mW h cm^{-3} at 133 mW cm^{-3}) [44], TiN//TiN (0.05 mW h cm^{-3} at 120 mW cm^{-3}) [45], and TiO_2@C//TiO_2@C (0.01 mW h cm^{-3} at 19 mW cm^{-3}) [46]. Such high energy and power density of our cells show great potential for practical energy storage applications.

4. Conclusions

To sum up, a facile synthetic approach has been developed here to directly assemble ternary $(Ni,Co)_{0.85}Se$ nanotubes on CFC for supercapacitor application. Its unique structure, superhydrophilic nature, and excellent conductivity enable a high areal capacitance of 2.33 F cm^{-2} at 4 mA cm^{-2}, showing clear advantages over the conventional supercapacitor electrodes (Supporting Table 1). Furthermore, an advanced asymmetric supercapacitor using metallic ternary $(Ni,Co)_{0.85}Se$ as positive electrode and porous graphene film as negative electrode has been successfully developed. Thanks to the highly porous nature, ideal electron and electrolyte transportation path, and considerable electrochemical activity of both positive and negative electrodes, our optimized $(Ni,Co)_{0.85}Se$//porous graphene film ASCs delivered a very high stack energy and power density, as well as robust stability.

Acknowledgments

Research reported in this publication has been supported by King Abdullah University of Science and Technology (KAUST).

Appendix A. Supplementary material

Supplementary data associated with this article can be found in the online version at http://dx.doi.org/10.1016/j.nanoen.2016.04.012.

References

[1] P. Simon, Y. Gogotsi, B. Dunn, Science 343 (2014) 1210–1211.
[2] J. Yan, Q. Wang, T. Wei, Z.J. Fan, Adv. Energy Mater. 4 (2014).
[3] Y. Gogotsi, P. Simon, Sci. Mag. 334 (2011) 917–918.
[4] J. Yan, Z. Fan, W. Sun, G. Ning, T. Wei, Q. Zhang, R. Zhang, L. Zhi, F. Wei, Adv. Funct. Mater. 22 (2012) 2632–2641.
[5] X.F. Lu, X.Y. Chen, W. Zhou, Y.X. Tong, G.R. Li, ACS Appl. Mater. Interface 7 (2015) 14843–14850.
[6] H. Xia, C. Hong, B. Li, B. Zhao, Z. Lin, M. Zheng, S.V. Savilov, S.M. Aldoshin, Adv. Funct. Mater. 25 (2015) 627–635.
[7] H. Gao, F. Xiao, C.B. Ching, H. Duan, Acs Appl. Mater. Interface 4 (2012) 2801–2810.
[8] C.X. Zhou, W. Yang, G.F. Zeng, Y. Lei, L. Gu, X.H. Xi, D. Xiao, Chem. Asian J. 10 (2015) 1745–1752.
[9] X. Yang, C. Cheng, Y. Wang, L. Qiu, D. Li, Science 341 (2013) 534–537.
[10] W. Chen, C. Xia, H. Alshareef, Nano Energy 15 (2015) 1–8.
[11] T. Brousse, M. Toupin, R. Dugas, L. Athouël, O. Crosnier, D. Bélanger, J Electrochem. Soc. 153 (2006) A2171–A2180.
[12] X.H. Xia, J.P. Tu, Y.J. Mai, X.L. Wang, C.D. Gu, X.B. Zhao, J Mater. Chem. 21 (2011) 9319–9325.
[13] U. Patil, K. Gurav, V. Fulari, C. Lokhande, O.S. Joo, J Power Sources 188 (2009) 338–342.
[14] C. Xia, W. Chen, X.B. Wang, M.N. Hedhili, N.N. Wei, H.N. Alshareef, Adv. Energy Mater. 5 (2015) 1401805.
[15] E. Frackowiak, V. Khomenko, K. Jurewicz, K. Lota, F. Beguin, J. Power Sources 153 (2006) 413–418.
[16] Q. Liao, N. Li, S. Jin, G. Yang, C. Wang, ACS Nano 9 (2015) 5310–5317.
[17] W. Chen, C. Xia, H.N. Alshareef, ACS Nano 8 (2014) 9531–9541.
[18] C. Xia, H.N. Alshareef, Chem. Mater. 27 (2015) 4661–4668.
[19] N. Kurra, C. Xia, M. Hedhili, H. Alshareef, Chem. Commun. 51 (2015) 10494–10497.
[20] L.F. Shen, J. Wang, G.Y. Xu, H.S. Li, H. Dou, X.G. Zhang, Adv. Energy Mater. 5 (2015) 1400977.
[21] J. Pu, T. Wang, H. Wang, Y. Tong, C. Lu, W. Kong, Z. Wang, Chempluschem 79 (2014) 577–583.
[22] L. Shen, L. Yu, H.B. Wu, X.Y. Yu, X. Zhang, X.W. Lou, Nat. Commun. 6 (2015) 6694.
[23] J.W. Xiao, L. Wan, S.H. Yang, F. Xiao, S. Wang, Nano Lett. 14 (2014) 831–838.
[24] S.J. Peng, L.L. Li, C.C. Li, H.T. Tan, R. Cai, H. Yu, S. Mhaisalkar, M. Srinivasan, S. Ramakrishna, Q.Y. Yan, Chem. Commun. 49 (2013) 10178–10180.
[25] C. Xia, P. Li, A.N. Gandi, U. Schwingenschlögl, H.N. Alshareef, Chem. Mater. 27 (2015) 6482–6485.
[26] X. Yang, J. Zhu, L. Qiu, D. Li, Adv. Mater. 23 (2011) 2833–2838.
[27] S. Chen, S.-Z. Qiao, ACS Nano 7 (2013) 10190–10196.
[28] C. Yuan, H.B. Wu, Y. Xie, X.W.D. Lou, Angew. Chem. Int. Ed. 53 (2014) 1488–1504.
[29] C. Xia, Q. Jiang, C. Zhao, M.N. Hedhili, H.N. Alshareef, Adv. Mater. 28 (2016) 77–85.
[30] A. Banerjee, S. Bhatnagar, K.K. Upadhyay, P. Yadav, S. Ogale, ACS Appl. Mater. Interface 6 (2014) 18844–18852.
[31] X.Y. Yan, X.L. Tong, L. Ma, Y.M. Tian, Y.S. Cai, C.W. Gong, M.G. Zhang, L.P. Liang, Mater. Lett. 124 (2014) 133–136.
[32] G.Q. Zhang, H.B. Wu, H.E. Hoster, M.B. Chan-Park, X.W. Lou, Energy Environ. Sci. 5 (2012) 9453–9456.
[33] L. Huang, D. Chen, Y. Ding, S. Feng, Z.L. Wang, M. Liu, Nano Lett. 13 (2013) 3135–3139.
[34] L. Yu, G. Zhang, C. Yuan, X.W.D. Lou, Chem. Commun. 49 (2013) 137–139.
[35] J.-W. Lang, L.-B. Kong, M. Liu, Y.-C. Luo, L. Kang, J. Solid State Electrochem. 14 (2010) 1533–1539.
[36] Z.-S. Wu, W. Ren, D.-W. Wang, F. Li, B. Liu, H.-M. Cheng, ACS Nano 4 (2010) 5835–5842.
[37] Z. Tang, Ch Tang, H. Gong, Adv. Funct. Mater. 22 (2012) 1272–1278.
[38] X. Wang, C. Yan, A. Sumboja, P.S. Lee, Nano Energy 3 (2014) 119–126.
[39] Y. Li, L. Cao, L. Qiao, M. Zhou, Y. Yang, P. Xiao, Y. Zhang, J. Mater. Chem. A 2 (2014) 6540–6548.
[40] D. Pech, M. Brunet, H. Durou, P. Huang, V. Mochalin, Y. Gogotsi, P.-L. Taberna, P. Simon, Nat. Nanotechnol. 5 (2010) 651–654.
[41] M.F. El-Kady, V. Strong, S. Dubin, R.B. Kaner, Science 335 (2012) 1326–1330.
[42] X. Lu, M. Yu, T. Zhai, G. Wang, S. Xie, T. Liu, C. Liang, Y. Tong, Y. Li, Nano Lett. 13 (2013) 2628–2633.
[43] X. Lu, M. Yu, G. Wang, T. Zhai, S. Xie, Y. Ling, Y. Tong, Y. Li, Adv. Mater. 25 (2013) 267–272.
[44] W. Zilong, Z. Zhu, J. Qiu, S. Yang, J. Mater. Chem. C 2 (2014) 1331–1336.
[45] X. Lu, G. Wang, T. Zhai, M. Yu, S. Xie, Y. Ling, C. Liang, Y. Tong, Y. Li, Nano Lett. 12 (2012) 5376–5381.
[46] H. Zheng, T. Zhai, M. Yu, S. Xie, C. Liang, W. Zhao, S.C.I. Wang, Z. Zhang, X. Lu, J. Mater. Chem. C 1 (2013) 225–229.

Chuan Xia is currently a PhD candidate of the Materials Science and Engineering program at KAUST. His research interests focus on the development of nanostructured chalcogenides and their applications.

Qiu Jiang obtained his bachelor degree from University of Science and Technology of China. He is currently a Master student of the Materials Science and Engineering program at KAUST. His research interests focus on fabricating On-Chip energy storage devices employing direct write and conventional lithography techniques.

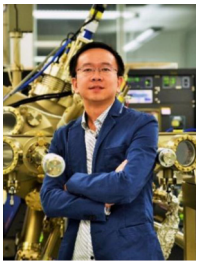

Dr. Chao Zhao is currently working on the growth and characterization of III-N materials, and device fabrication for optoelectronic applications at KAUST. He received his Ph.D. in Microelectronics and Solid state electronics from Chinese Academy of Sciences in 2009. From 2009–2015, he was working as a Research Scientist in Core Labs on Electron Microscopy, X-Ray Diffraction and deposition systems.

Dr. Pierre M. Beaujuge is Faculty in the Materials Sciences & Engineering and in the Chemical Sciences Programs at King Abdullah University of Science & Technology (KAUST). He is also member of the Solar & Photovoltaics Engineering Research Center (SPERC) at KAUST. He received his Ph.D. from University of Florida in 2009, and worked as a Post-Doctoral Associate at University of California, Berkeley (2009–2010) and in the Materials Sciences Division of Lawrence Berkeley National Laboratory (2010–2011).

Dr. Husam N. Alshaeef a Professor of Materials Science & Engineering at King Abdullah University of Science & Technology (KAUST). He obtained his PhD at North Carolina State University, USA. Following nearly 10 years of experience in the semiconductor industry, he joined KAUST in 2009. His group is interested in developing semiconductor nanomaterials for electronics and energy applications.